Electronic Supplementary Information

In situ fabricated nickel vanadate/N-doped reduced graphene oxide hybrid as an advanced electrocatalyst in alkaline hydrogen evolution reaction

Ayon Karmakar[a] and Suneel Kumar Srivastava*[ab]

[a]*Inorganic Materials and Nanocomposite Laboratory, Department of Chemistry, Indian Institute of Technology Kharagpur, Kharagpur 721302, India.*

[b]*School of Energy Science and Engineering, Indian Institute of Technology Kharagpur, Kharagpur 721302, India.*

*E-mail: sunil111954@yahoo.co.uk

Experimental section

Materials

Sulphuric acid (H_2SO_4), phosphoric acid (H_3PO_4), potassium permanganate ($KMnO_4$), hydrogen peroxide (H_2O_2), hydrochloric acid (HCl), nickel chloride hexahydrate ($NiCl_2.6H_2O$), urea ($CO(NH_2)_2$), ethylene glycol ($C_2H_6O_2$) and pure graphite powder (Micro 850 grade) were procured from Merck India and Asbury Carbons respectively. In addition, potassium hydroxide (KOH), ammonium metavanadate (NH_4VO_3) and Pt/C (20 wt.%) were purchased from SRL Chemicals and Sigma-Aldrich respectively. All these reagents were analytical grade and used without further purification. Distilled water was used throughout all the experiments.

Synthesis of Graphene Oxide

Graphene oxide (GO) was prepared by modified Hummers' method.[1] In this method, 0.5 gm graphite flakes was added to in a 500 mL beaker containing the mixture of concentrated H_2SO_4/H_3PO_4 (9:1, v/v, 70 ml) maintained on an ice bath followed by continuous stirring for 15 min. Subsequently, 1.5 gm of $KMnO_4$ (3 equivalent) was slowly added and the mixture was stirred for another 1 hr. After 1 hr, 40 mL of cold water was added very slowly to the previous mixture at room temperature. This is followed by the addition of 240 mL hot distilled water and stirred for 40 min. Subsequently, 5 mL of H_2O_2 was added to the earlier mixture and further stirred for 30 minutes. The product obtained in this manner was washed by HCl solution (5%) followed by distilled water until the pH of the supernatant liquid becomes neutral and finally dried at 60 °C in an air oven for 2 days.

Fabrication of Nickel Vanadate/NRGO Hybrid

40 mg GO was dispersed ultrasonically for 1 hour in 60 mL mixed solvent (water/Ethylene glycol:1/1) in a 250 mL round bottom flask (RB) and then centrifuged to remove the unexfoliated portions. Subsequently, 3 mmol $NiCl_2.6H_2O$ was added to the previous

exfoliated GO dispersion. Following this, earlier dispersion was magnetically stirred for 1 h in order to achieve good electrostatic attachment between negatively charged GO and Ni^{2+} ions. Subsequently, 2 mmol NH_4VO_3 dissolved in 20 mL mixed solvent was added to earlier dispersion maintained at room temperature. Thereafter, 12 mmol urea was added to this and subjected to stirring for 30 min and reflexed in an oil-bath at ~140 °C for 6 h. After cooling down naturally, pH of the mixture was found to be ~9 and precipitate formed at the bottom of RB was filtered, washed several times with water/ethanol and dried at 60 °C for 12 h. Finally, brownish powdered product obtained in this manner was collected and referred as NV/NRGO2. In addition, two more samples were prepared in the same fashion by varying the amount of GO, named NV/NRGO1 (using 20 mg GO) and NV/NRGO3 (using 60 mg GO). The pure nickel vanadate (NV) was also fabricated in absence of GO following the similar procedure for comparing its electrochemical performance with earlier prepared hybrid samples. Further, NRGO, NV/RGO, NiO, and V_2O_5 were also fabricated and the fabrication procedures are described below.

Preparation of NRGO

NRGO was prepared in a similar manner as $Ni_3V_2O_8$/NRGO hybrids in absence of nickel and vanadium sources and keeping all other reaction parameters unchanged.

Preparation of $Ni_3V_2O_8$/RGO hybrid

$Ni_3V_2O_8$/RGO (NV/RGO) hybrid was fabricated in the same fashion as described for NV/NRGO2 in absence of urea and other parameters remained unaltered. The pH of the final reaction mixture was adjusted to 9 by dropwise addition of 0.5 (M) NaOH before subjecting to reflux.

Preparation of NiO

5 mmol $NiCl_2.6H_2O$ dissolved in 60 mL mixed solvent (water/Ethylene glycol:1/1) in a 250 mL RB and 12 mmol urea was dissolved in another 20 mL mixed solvent. Subsequently, both these two solutions were mixed together and refluxed in an oil-bath at ~140 °C for 6 h. Thereafter, the reaction mixture was cooled naturally to room temperature and the light green colored precipitate was filtered, washed and dried at 60 °C for 12 h. Further, the precipitate was calcined at 400 °C for 2 h in air and final black colored powdered product was collected.

Preparation of V_2O_5

In order to prepare V_2O_5, 5 mmol NH_4VO_3 dissolved in 80 mL mixed solvent (water/Ethylene glycol:1/1) at 80 °C and a pale yellow colored solution was obtained. Subsequently, 12 mmol urea was added to the above solution and the final solution was refluxed at 140 °C for 12 h. Then the reaction mixture was cooled down to room temperature and precipitate formed at boot was filtered, washed and dried at 60 °C. The dried product was calcined at 500 °C for 2 h in a muffle furnace in air atmosphere and golden yellow colored powders were collected as the final product.

Characterization Techniques

X-ray diffraction (XRD) of the samples were carried out on Bruker D8 Advance with Cu Kα radiation in the scan ranges of 2θ = 10°–70°. Thermogravimetric analysis was performed on a Q20 thermogravimetric analyzer (TA Instruments) in the temperature range of 30–800 °C at a heating rate of 10 °C min^{-1} in air atmosphere. Carl-Zeiss MERLIN field emission scanning electron microscopy (FESEM), FEI-TECNAI-G2 Transmission electron microscopy (TEM) and JEOL JEM-2100F scanning transmission electron microscopy (STEM) equipped with energy dispersive X-ray spectroscopy (EDX) were employed to identify the morphology, microstructure, and elemental composition of the prepared samples. Inductively coupled plasma mass spectrometry was conducted using an iCAP Q ICP-MS (Thermo Scientific).

Raman analyses were carried out in an Optical Microscope BX41 (Olympus, Japan) T64000 (Jobin Yvon Horiba, France) spectrometer equipped with argon-krypton mixed ion gas laser 2018 RM (Spectra Physics, USA) at an excitation wavelength of 514.5 nm in the frequency range of 200–2000 cm^{-1}. X-ray photoelectron spectroscopy (XPS) of the samples were examined using PHI 5000 Versa Probe II (ULVAC–PHI, INC, Japan) coupled with a micro-focused (100 μm, 25 W, 15 kV) monochromatic Al Kα source ($h\nu$ = 1486.6 eV).

Electrochemical characterization

The working electrode (~1.0 cm^2) is prepared by coating slurry on a Ni-foil (NF). For this purpose, NF was initially cleaned using 6 M HCl, water, and ethanol while subjecting it to sonication for 10 min and dried at 60 °C for 15 min in vacuum oven. Following this, it was coated with the slurry consisting of active catalyst, carbon black, and PVDF (8:1:1) in N-methyl pyrolidone (NMP). Subsequently, electrochemical measurements of catalysts (~1.84 mg cm^{-2}) were performed with *iR*-compensation on CHI7086E electrochemical work station (CH Instruments Inc., USA) in a standard three electrode configuration using saturated calomel electrode (SCE) from CHI, graphite sheet, and catalyst coated Ni-foil as reference, counter, and working electrode, respectively. In all these experiments, freshly prepared 1.0 M KOH was used as electrolyte. The potentials in our work are represented with respect to reversible hydrogen electrode (RHE) according to the following equation: $E_{RHE} = E_{SCE} + 1.006$ (Fig. S1). The linear sweep voltammetry (LSV) of the samples were recorded at 5 mV s^{-1} in the potential range of -0.5 – 0.05 V versus RHE for HER. But, prior to the LSV, catalysts were activated for HER in the above potential window by performing cyclic voltammetry (CV) measurements at a scan rate of 50 mV s^{-1} for 100 cycles. Thereafter, CV of different catalysts were performed at different scan rates (10–100 mV s^{-1}) in the potential range of 0.106 – 0.206 V (non-Faradic region) versus RHE to measure electrochemical double layer capacitance (C_{dl}). The electrochemical impedance spectroscopy (EIS) was also

employed to investigate the charge transfer resistance (R_{ct}) at -0.244 V in the frequency range of 100 kHz–10^{-1} Hz with AC amplitude of 5 mV. In order to check the long term stability of the catalysts, galvanostatic measurements were performed at 10 mA cm^{-2} current density for 12 h. Subsequently, LSV was recorded before and after 1000 potential cycling in the cathodic region corresponding to HER.

Calibration of SCE and conversion to RHE

The calibration of SCE (CHI150) with respect to RHE was performed in H_2-saturated 1.0 M KOH electrolyte using two Pt-wires as working and counter electrodes. LSV was run at a scan rate of 5 mV s^{-1} and the potential at zero current is considered as the thermodynamic potential for the hydrogen electrode reactions (Fig. S1). It is noted that, H_2 purging was continued throughout the measurement. Thus, in 1.0 M KOH, $E_{RHE} = E_{SCE} + 1.006\ V$.

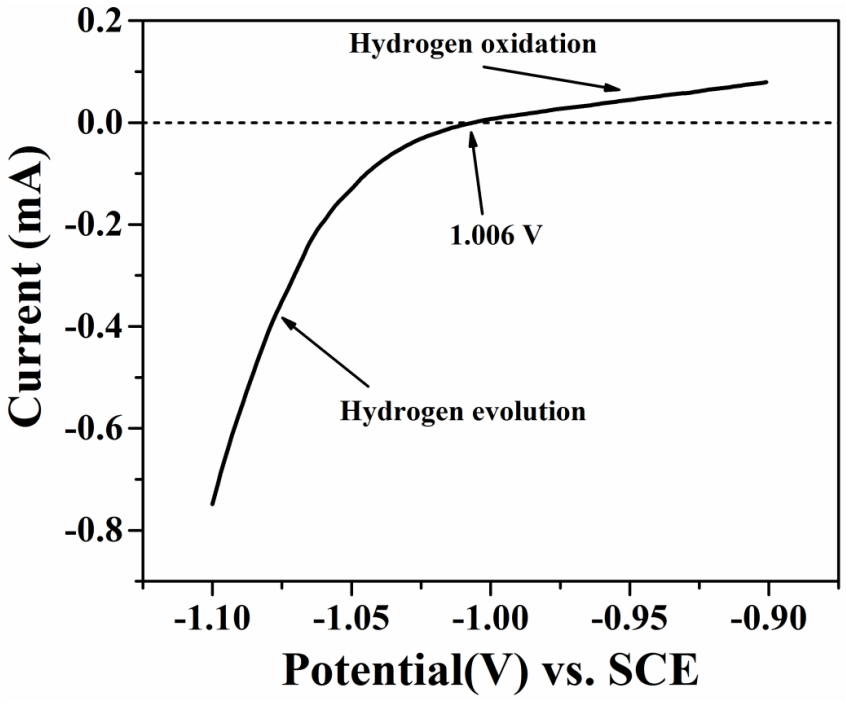

Figure S1. Calibration of SCE with respect to RHE.

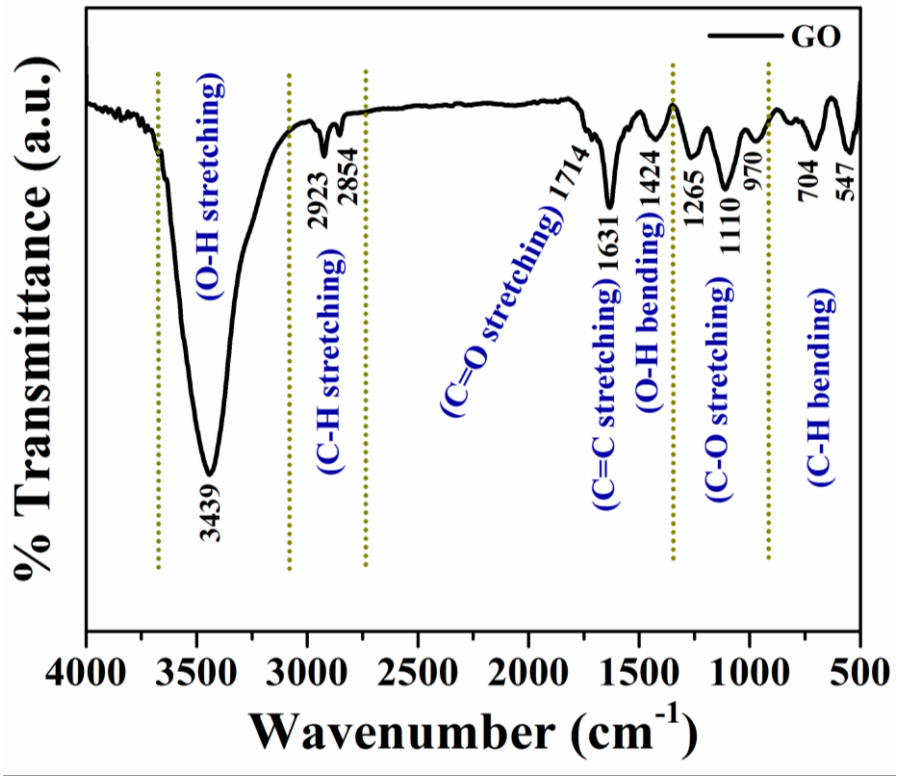

Figure S2. FTIR spectrum of graphene oxide (GO).

Thermogravimetric analysis

Thermal stability behaviour of NV and composition of NV/NRGO hybrid samples has been investigated by thermogravimetric analysis (air) in the temperature range of 30–800 °C and the corresponding findings are displayed in Figure S3. All the samples underwent an initial weight loss upto ~230 °C, owing to the expulsion of interlayer/adsorbed water molecules.[2,3] It is noted that NV sample attain stability above ~400 °C and ~84.7 % of its initial amount remains at 800 °C. In contrast, hybrid samples showed further sharp weight loss above ~450 °C and followed the order: NV/NRGO1 < NV/NRGO2 < NV/NRGO3. In view of this, reduced graphene oxide undergoes bulk pyrolysis of carbon skeleton at 400 °C and nearly complete decomposition was observed above 500 °C in the previous reports.[4] Accordingly, amount of NRGO present in NV/NRGO1, NV/NRGO2, and NV/NRGO3 hybrids were calculated by considering the fact that entire NRGO has completely pyrolysed (weight loss ~100%) above 500 °C and found to be ~3.3, 5.6, and 6.6 wt.%, respectively.

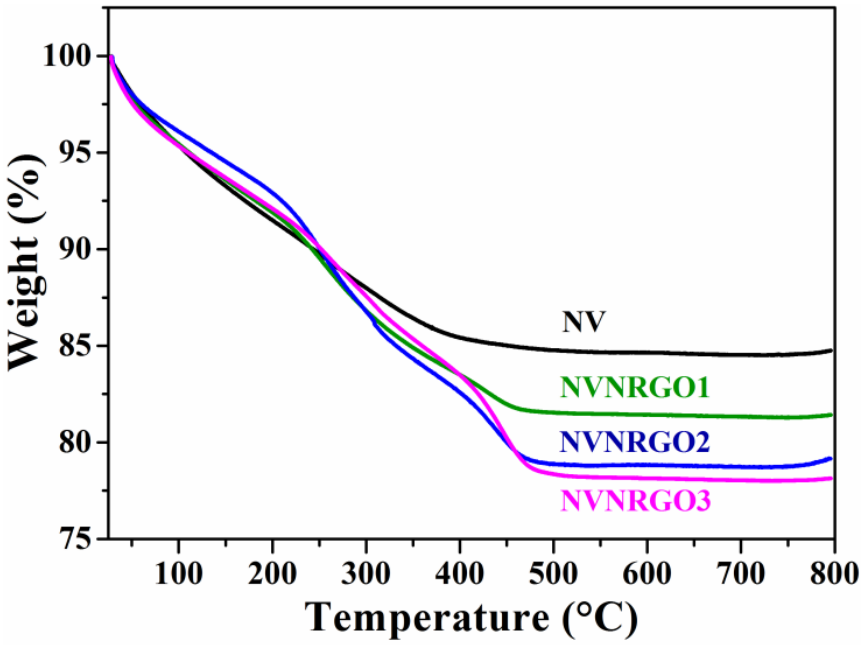

Figure S3. TGA curve of pure NV and NV/NRGO hybrid samples.

Table S1. Amount of Carbon, Hydrogen, and Nitrogen present in $Ni_3V_2O_8$@NRGO hybrids, obtained from CHN analysis.

Samples	Carbon (%)	Hydrogen (%)	Nitrogen (%)
NV/NRGO1	3.21	1.55	0.29
NV/NRGO2	5.57	1.38	0.40
NV/NRGO3	6.07	1.55	0.52

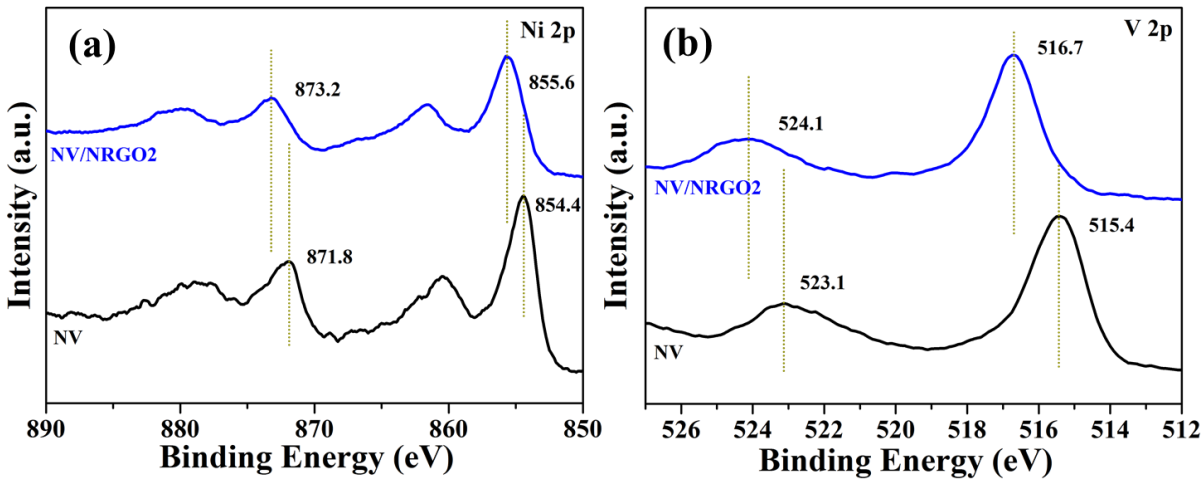

Figure S4. High resolution (a) Ni 2p and (b) V 2p spectra of NV and NV/NRGO2.

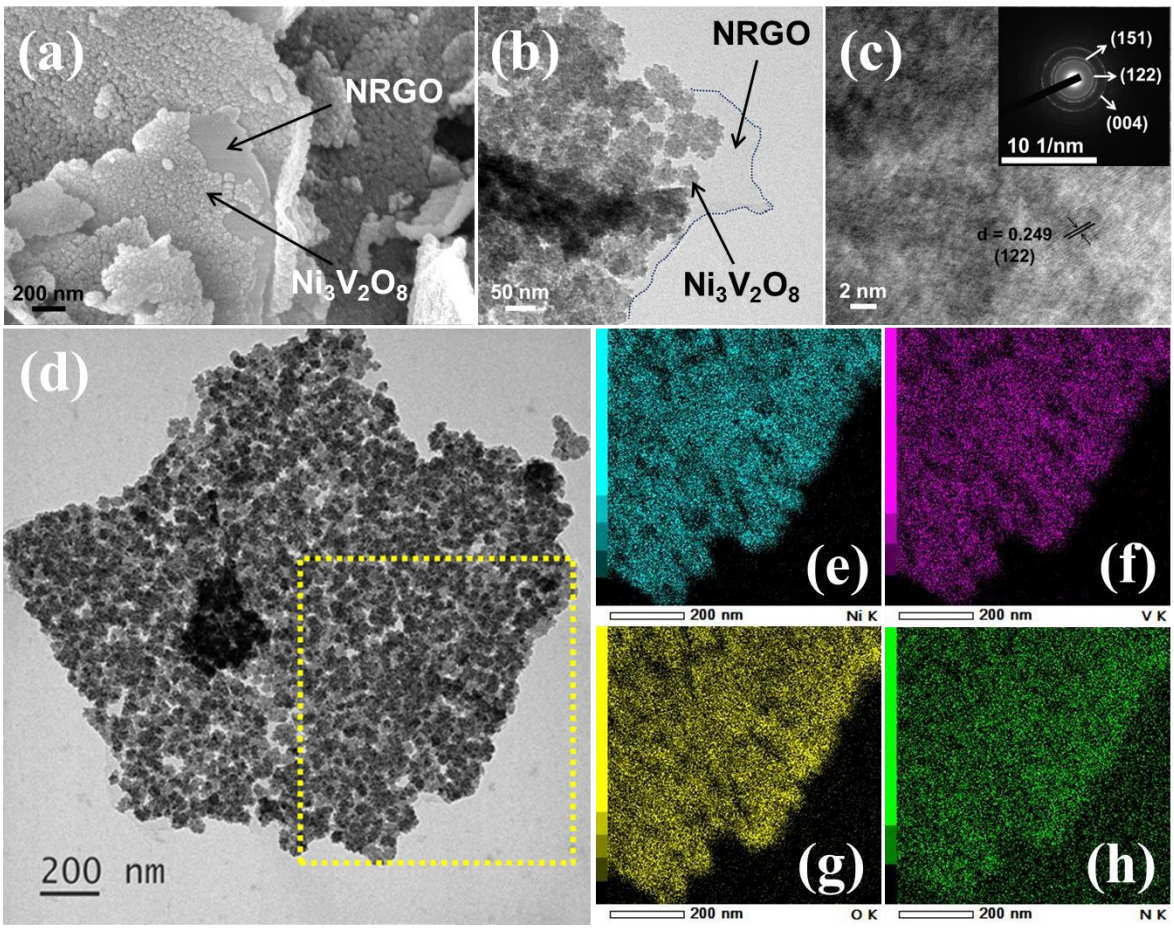

Figure S5. (a) FESEM, (b) TEM, and (c) HRTEM (SAED at inset), (d) STEM and corresponding (e) Ni, (f) V, (g) O, and (h) N elemental mapping images of NV/NRGO2, respectively.

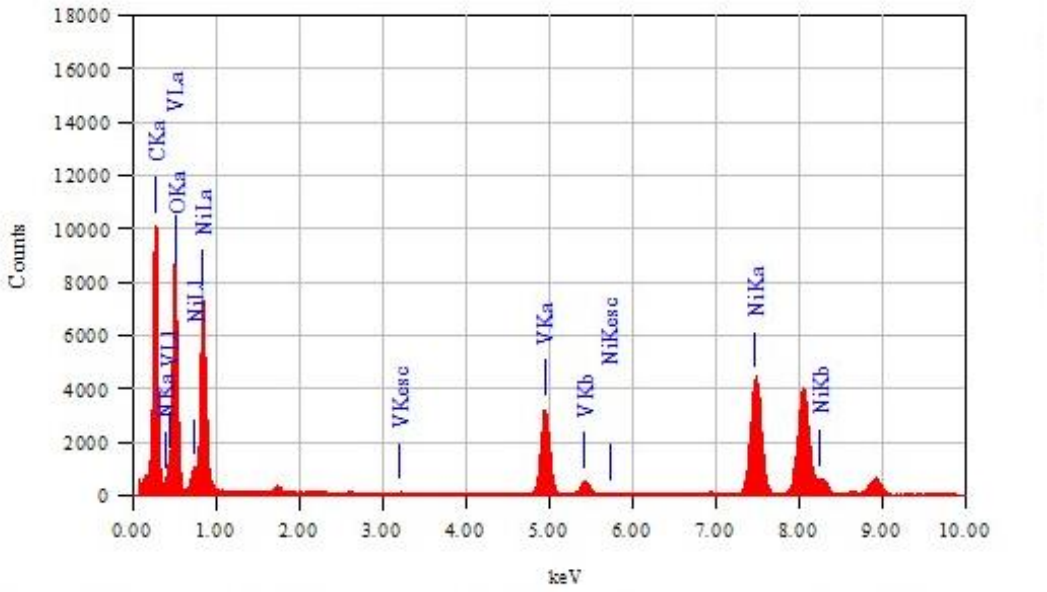

Thin Film Standardless Standardless Quantitative Analysis
Fitting Coefficient : 0.2920

Element	(keV)	Mass%	Counts	Sigma	Atom%	Compound
C K	0.277	49.82	52506.79	0.18	72.24	
N K		ND			ND	
O K	0.525	15.57	38715.95	0.12	16.95	
V K	4.949	11.84	38336.18	0.12	4.05	
Ni K (Ref.)	7.471	22.77	57608.79	0.19	6.76	
Total		100.00			100.00	

Figure S6. EDX spectrum of NV/NRGO2.

Table S2. Elemental analysis of NV/NRGO2 by ICP-MS.

Sample	Ni	V	Ni : V (molar ratio)
NV/NRGO2	230 ppm	125 ppm	1.59

Table S3. HER overpotentials (η) at different current densities of Pt/C, NV, NRGO, NV/RGO, and NV/NRGO hybrids in 1.0 M KOH.

Samples	η_{10} **(mV)**	η_{50} **(mV)**	η_{100} **(mV)**
Pt/C	16	43	59
NV	97	140	163
NRGO	194	239	259
NV/RGO	236	304	333
NV/NRGO1	94	154	187
NV/NRGO2	43	97	134
NV/NRGO3	81	131	160

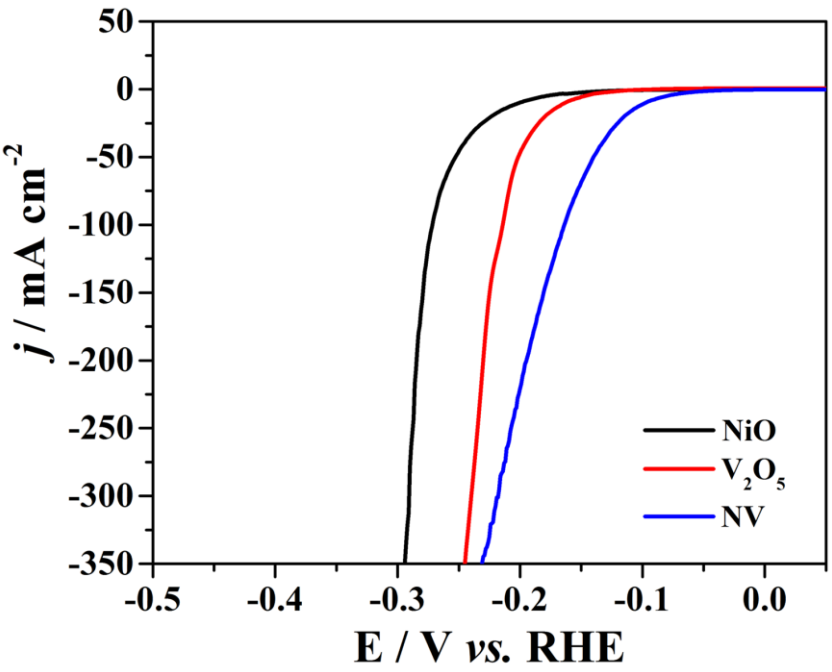

Figure S7. LSV polarization curves for HER at 5 mV s^{-1} of NiO, V_2O_5, and NV in 1.0 M KOH with *iR*-correction.

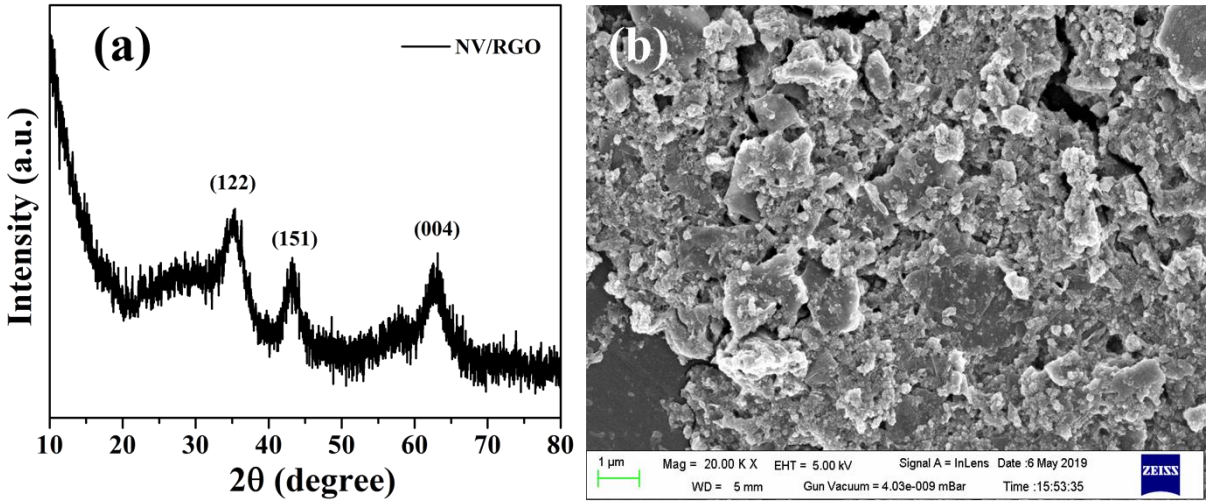

Figure S8. (a) XRD pattern and (b) FESEM image of NV/RGO.

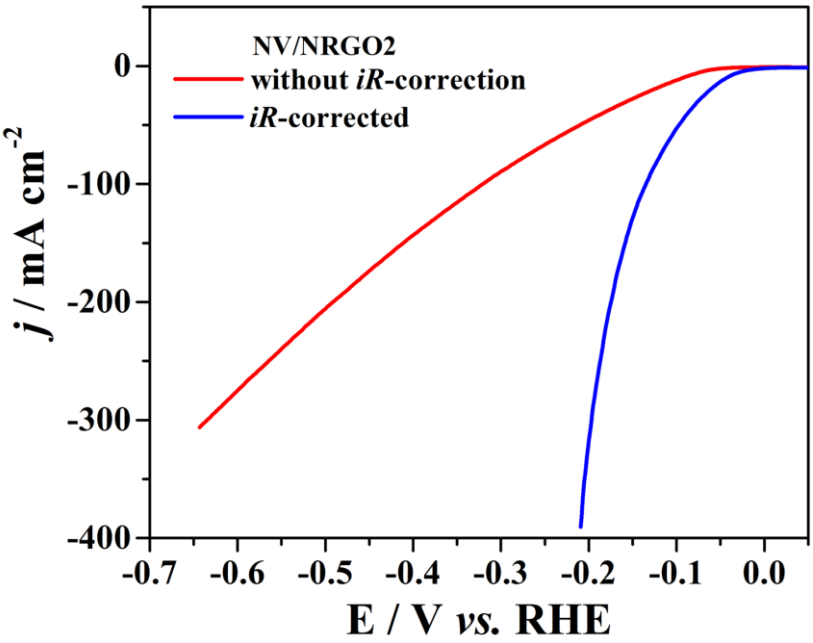

Figure S9. LSV curves of NV/NRGO2 at 5 mV s^{-1} with and without *iR*-correction.

Turnover frequency (TOF) calculation

TOF (s^{-1}) was calculated according to the equation as stated below:[5]

$$TOF = \frac{|j|S_{geo}}{2Fn}$$

where $|j|$ is the current density (A cm^{-2}), S_{geo} is the geometric surface area of the working electrode (1 cm^2), ½ is used as HER involves 2 electrons per mole of H_2, F is the Faraday constant (96485 C mol^{-1}), and n is number of active sites (mol) considering that all the metal atoms present in each sample are electrocatalytically active. In order to calculate number of active sites (n), cyclic votltammograms (CV) were recorded -0.9 to 0.8 V at 10 mV s^{-1} in 1.0 M KOH. The absolute components of the voltammetric charges (cathodic and anodic) during one CV cycle were measured. Subsequently, considering one electron redox process, this absolute charge was divided by two and then divided by the Faraday constant.[6]

Equivalent circuit in Nyquist plot

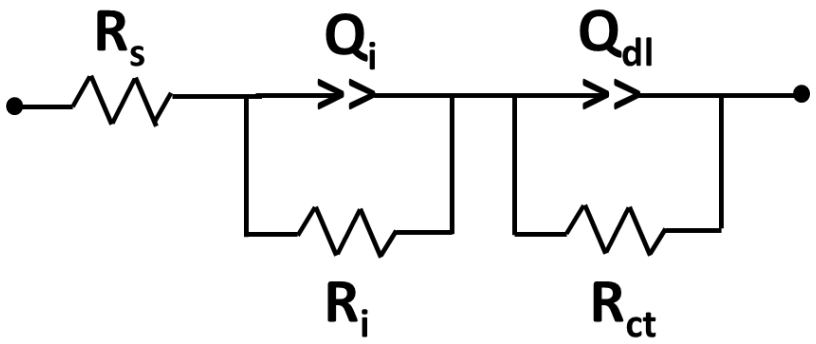

$\boldsymbol{R_s}$: Electrolyte resistance

$\boldsymbol{Q_i}$ and $\boldsymbol{R_i}$: Constant phase element and intrinsic/contact resistance of the catalyst respectively.

$\boldsymbol{Q_{dl}}$ and $\boldsymbol{R_{ct}}$: Constant phase element of double layer capacitor and charge transfer resistance at the catalyst–electrolyte interface respectively.

Electrochemical active surface area (ECSA) calculation

The dependency of CV on scan rate (10–100 mV sec^{-1}) of all samples is displayed in Figure S10. Subsequently, charging current (i_c) was plotted against scan rate (ν) at the potential corresponding to 0.156 V (Fig. S11a) and related to the following equation:[7]

$$i_c = \nu C_{dl}$$

The slope of the linear plots corresponds to electrochemical double layer capacitance (C_{dl}) and related to electrochemical active surface area (ECSA) as:[8,9]

$$ECSA = C_{dl}/C_s$$

where C_s is the specific double-layer capacitance of a smooth catalyst surface and considered as 0.04 mF cm^{-2} for all the prepared catalysts.[8]

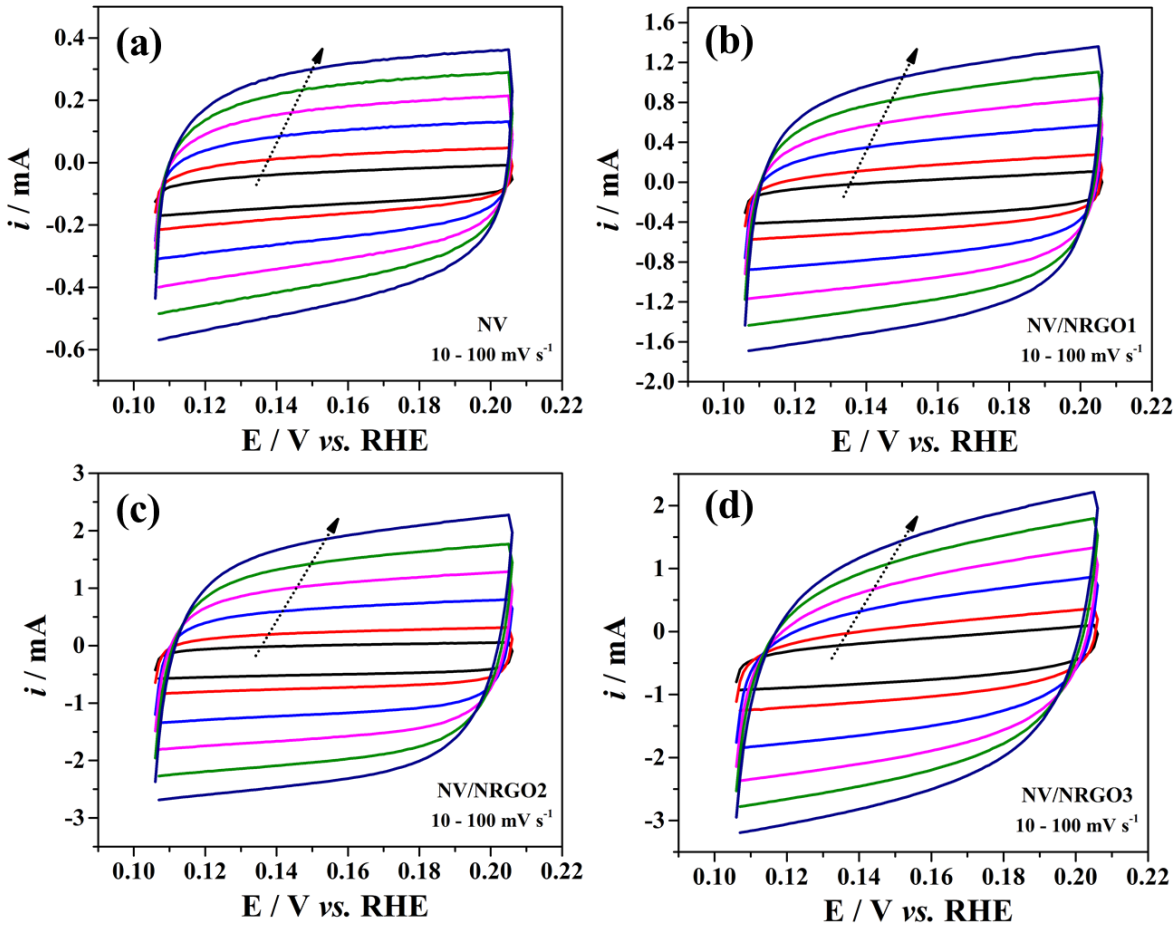

Figure S10. CV curves for C_{dl} at different scan rates (10 – 100 mV s^{-1}) of (a) NV, (b) NV/NRGO1, (c) NV/NRGO2, and (d) NV/NRGO3, respectively.

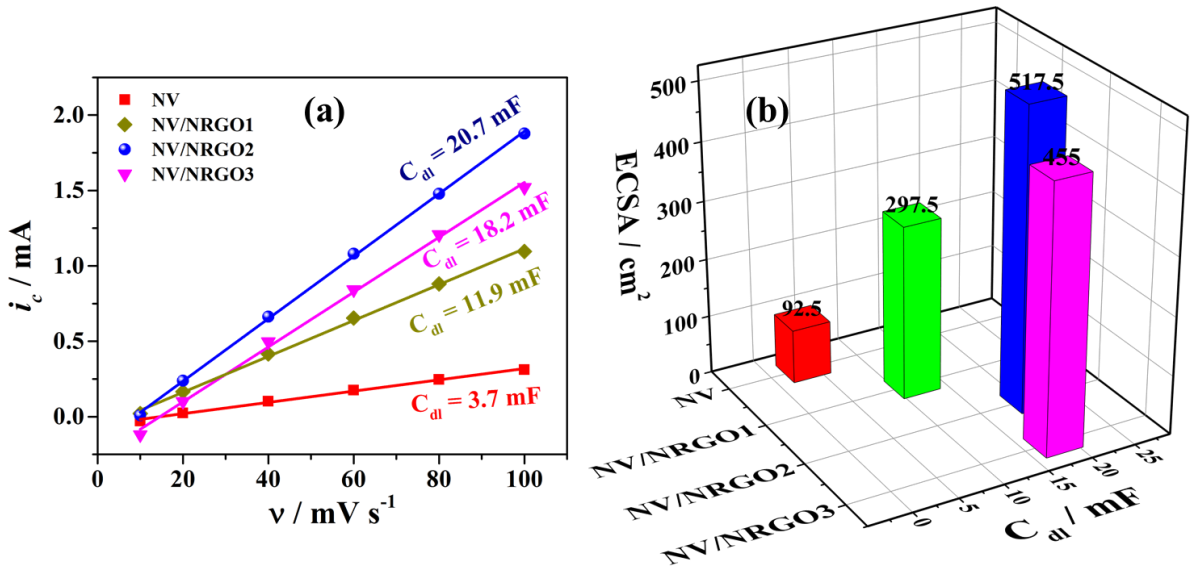

Figure S11. (a) Electrochemical double layer capacitance (C_{dl}) at 0.156 V vs. RHE and (b) electrochemical active surface area (ECSA) of NV, NV/NRGO1, NV/NRGO2, and NV/NRGO3, respectively.

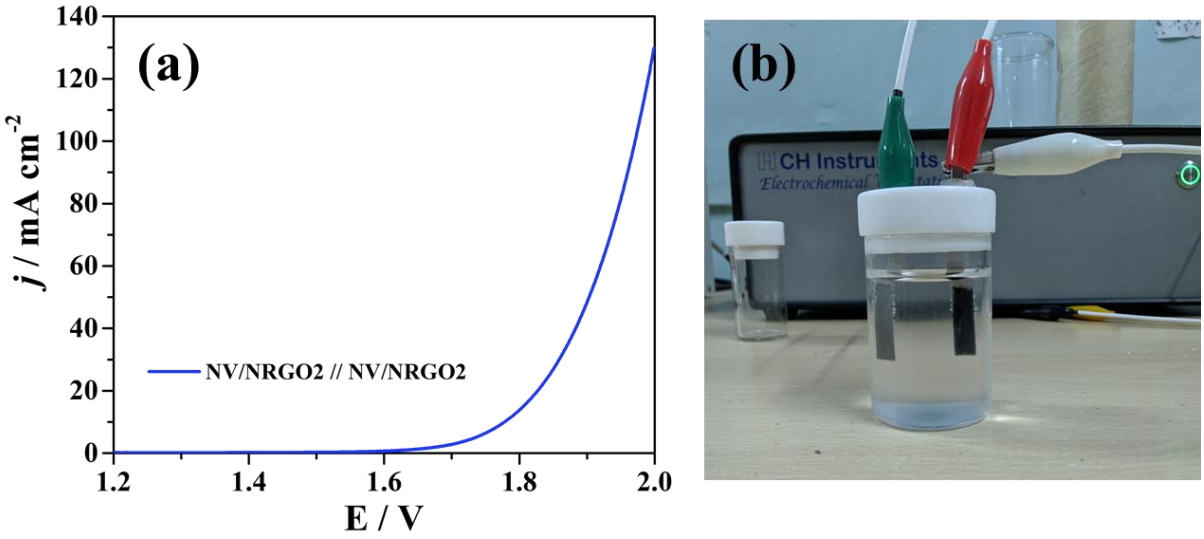

Figure S12. (a) Polarization curve and (b) digital image of two electrode configuration using NV/NRGO2 as both anode and cathode in 1.0 M KOH.

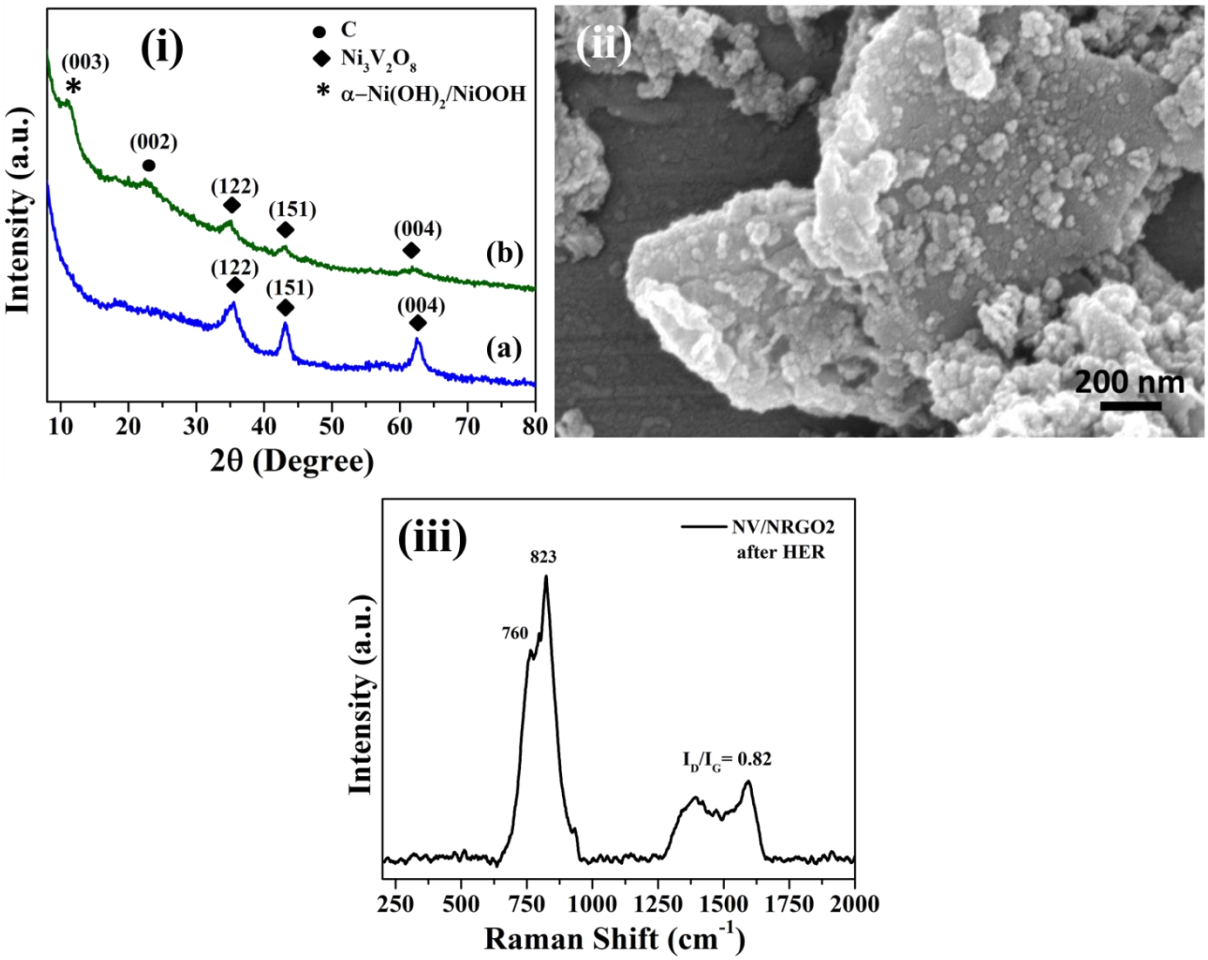

Figure S13. (i) XRD pattern of NV/NRGO2 before HER tests (a) and after durability tests (b). (ii) FESEM image and (iii) Raman spectrum of NV/NRGO2 after HER durability tests.

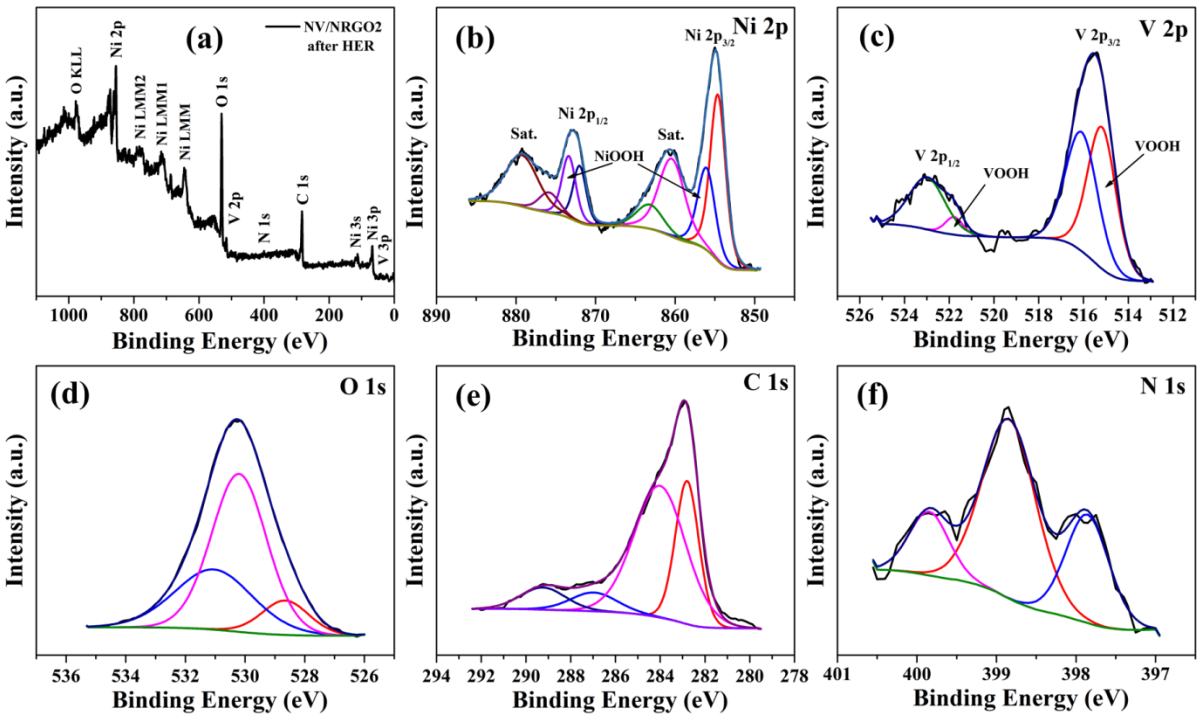

Figure S14. (a) XPS survey spectrum and high-resolution XPS spectra of (b) Ni 2p, (c) V 2p, (d) O 1s, (e) C 1s, and (f) N 1s regions of NV/NRGO2 after HER stability tests.

Table S4. Comparison of electrocatalytic HER activity in alkaline medium with few available literature.

Catalyst	**Electrolyte**	**η_{10} (mV)**	**Tafel slope (mV dec^{-1})**	**References**
$P_{8.6}$-Co_3O_4/NF	1.0 M KOH	97	86	[10]
Nest-like NiCoP	1.0 M KOH	62	68.2	[11]
Cu NDs/Ni_3S_2 NTs-CFs	1.0 M KOH	128	76.2	[5]
Ni_3N@CQDs	1.0 M KOH	69	108	[12]
$Co(OH)_2$@PANI HNSs/NF	1.0 M NaOH	88	91.6	[13]
N,P-Doped Mo_2C@C Nanospheres	1.0 M KOH	47	71	[14]
Mo_2C/N-doped carbon microflowers	1.0 M KOH	100	65	[15]
$Fe_{17.5\%}$-Ni_3S_2/NF	1.0 M KOH	47	95	[16]
Co_3S_4 porous nanosheets	1.0 M KOH	63	58	[17]
Ni_3P MPs	1.0 M KOH	291	119	[18]
Ni_2P/Ni/NF	1.0 M KOH	98	72	[19]
Reduced $NiCo_2O_4$	1.0 M KOH	135	52	[20]
Holey NiCoP NS	1.0 M KOH	58	57	[21]
CoO_x@CN	1.0 M KOH	232	115	[22]
2D MoS_2 confined $Co(OH)_2$	1.0 M KOH	89	53	[23]
Co_2P@NPG	1.0 M KOH	165	96	[24]
NiO/Ni-CNT	1.0 M KOH	80	82	[25]
VOOH hollow nanospheres	1.0 M KOH	164	104	[26]
$Ni_3(VO_4)_2$@$NiCo_2O_4$/NF	1.0 M KOH	113	101	[8]
$CoMoO_4$ NWA/Ti	1.0 M KOH	81	63	[27]
Ni–Mn_3O_4/NF	1.0 M KOH	91	110	[28]
P-Co_3O_4	1.0 M KOH	120	52	[29]
$NiCo_2O_4$ hollow microcuboids	1.0 M NaOH	110	49.7	[30]
$NiFeO_x$/CFP	1.0 M KOH	88	150.2	[31]
β-$Ni(OH)_2$/Pt	1.0 M KOH	108	39	[32]
Co_3N plate	1.0 M KOH	230	101.6	[33]
Ni_3N/NF	1.0 M KOH	121	109	[34]
Sr_2RuO_4	1.0 M KOH	61	51	[35]
Pt-Ni alloy	0.1 M KOH	82	-	[36]
N–Co–C/RGO	1.0 M KOH	130	77	[37]
Ru-Ru2P@PC	1.0 M KOH	43.4	35.1	[38]
Ni3N@VN–NF	1.0 M KOH	56	47	[39]
Pt/C (20 wt.%)	**1.0 M KOH**	**16**	**30.3**	**This work**
$Ni_3V_2O_8$/NRGO (5.6 wt.%)	**1.0 M KOH**	**43**	**54.8**	**This work**

References

1 D. C. Marcano, D. V. Kosynkin, J. M. Berlin, A. Sinitskii, Z. Sun, A. Slesarev, L. B. Alemany, W. Lu and J. M. Tour, *ACS Nano*, 2010, **4**, 4806–4814.

2 R. Kumar, P. K. Gupta, P. Rai and A. Sharma, *New J. Chem.*, 2018, **42**, 1243–1249.

3 R. Sahoo, A. Pal and T. Pal, *J. Mater. Chem. A*, 2016, **4**, 17440–17454.

4 S. Azizighannad and S. Mitra, *Sci. Rep.*, 2018, **8**, 10083.

5 J. X. Feng, J. Q. Wu, Y. Tong and G. R. Li, *J. Am. Chem. Soc.*, 2018, **140**, 610–617.

6 J. Zhang, T. Wang, P. Liu, Z. Liao, S. Liu, X. Zhuang, M. Chen, E. Zschech and X. Feng, *Nat. Commun.*, 2017, **8**, 1–8.

7 A. Karmakar and S. K. Srivastava, *ACS Appl. Mater. Interfaces*, 2017, **9**, 22378–22387.

8 X. Shang, J. Q. Chi, S. S. Lu, B. Dong, Z. Z. Liu, K. L. Yan, W. K. Gao, Y. M. Chai and C. G. Liu, *Electrochim. Acta*, 2017, **256**, 100–109.

9 A. Maiti and S. K. Srivastava, *J. Mater. Chem. A*, 2018, **6**, 19712–19726.

10 Z. Wang, H. Liu, R. Ge, X. Ren, J. Ren, D. Yang, L. Zhang and X. Sun, *ACS Catal.*, 2018, **8**, 2236–2241.

11 C. Du, L. Yang, F. Yang, G. Cheng and W. Luo, *ACS Catal.*, 2017, **7**, 4131–4137.

12 M. Zhou, Q. Weng, Z. I. Popov, Y. Yang, L. Y. Antipina, P. B. Sorokin, X. Wang, Y. Bando and D. Golberg, *ACS Nano*, 2018, **12**, 4148–4155.

13 J. X. Feng, L. X. Ding, S. H. Ye, X. J. He, H. Xu, Y. X. Tong and G. R. Li, *Adv. Mater.*, 2015, **27**, 7051–7057.

14 Y. Y. Chen, Y. Zhang, W. J. Jiang, X. Zhang, Z. Dai, L. J. Wan and J. S. Hu, *ACS Nano*, 2016, **10**, 8851–8860.

15 Y. Huang, Q. Gong, X. Song, K. Feng, K. Nie, F. Zhao, Y. Wang, M. Zeng, J. Zhong and Y. Li, *ACS Nano*, 2016, **10**, 11337–11343.

16 G. Zhang, Y. S. Feng, W. T. Lu, D. He, C. Y. Wang, Y. K. Li, X. Y. Wang and F. F. Cao, *ACS Catal.*, 2018, **8**, 5431–5441.

17 C. Zhang, Y. Shi, Y. Yu, Y. Du and B. Zhang, *ACS Catal.*, 2018, **8**, 8077–8083.

18 A. B. Laursen, R. B. Wexler, M. J. Whitaker, E. J. Izett, K. U. D. Calvinho, S. Hwang, R. Rucker, H. Wang, J. Li, E. Garfunkel, M. Greenblatt, A. M. Rappe and G. C. Dismukes, *ACS Catal.*, 2018, **8**, 4408–4419.

19 B. You, N. Jiang, M. Sheng, M. W. Bhushan and Y. Sun, *ACS Catal.*, 2016, **6**, 714–721.

20 S. Peng, F. Gong, L. Li, D. Yu, D. Ji, Z. Hu, Z. Zhang, S. Chou, T. Zhang, Y. Du and S. Ramakrishna, *J. Am. Chem. Soc.*, 2018, **140**, 13644−13653.

21 Z. Fang, L. Peng, Y. Qian, X. Zhang, Y. Xie, J. J. Cha and G. Yu, *J. Am. Chem. Soc.*, 2018, **140**, 5241–5247.

22 H. Jin, J. Wang, D. Su, Z. Wei, Z. Pang and Y. Wang, *J. Am. Chem. Soc.*, 2015, **137**, 2688–2694.

23 Y. Luo, X. Li, X. Cai, X. Zou, F. Kang, H.-M. Cheng and B. Liu, *ACS Nano*, 2018, **12**, 4565–4573.

24 M. Zhuang, X. Ou, Y. Dou, L. Zhang, Q. Zhang, R. Wu, Y. Ding, M. Shao and Z. Luo, *Nano Lett.*, 2016, **16**, 4691–4698.

25 M. Gong, W. Zhou, M. C. Tsai, J. Zhou, M. Guan, M. C. Lin, B. Zhang, Y. Hu, D. Y. Wang, J. Yang, S. J. Pennycook, B. J. Hwang and H. Dai, *Nat. Commun.*, 2014, **5**, 4695.

26 H. Shi, H. Liang, F. Ming and Z. Wang, *Angew. Chem., Int. Ed.*, 2017, **56**, 573–577.

27 J. Zhao, X. Ren, H. Ma, X. Sun, Y. Zhang, T. Yan, Q. Wei and D. Wu, *ACS Sustain. Chem. Eng.*, 2017, **5**, 10093–10098.

28 X. Li, P. F. Liu, L. Zhang, M. Y. Zu, Y. X. Yang and H. G. Yang, *Chem. Commun.*, 2016, **52**, 10566–10569.

29 S. Wang, Z. Xiao, Y. Wang, Y. C. Huang, Z. Wei, C. L. Dong, J. Ma, S. Shen and Y. Li, *Energy Environ. Sci.*, 2017, **10**, 2563–2569.

30 X. Gao, H. Zhang, Q. Li, X. Yu, Z. Hong, X. Zhang, C. Liang and Z. Lin, *Angew. Chem., Int. Ed.*, 2016, **55**, 6290–6294.

31 H. Wang, H. W. Lee, Y. Deng, Z. Lu, P. C. Hsu, Y. Liu, D. Lin and Y. Cui, *Nat. Commun.*, 2015, **6**, 7261.

32 X. Yu, J. Zhao, L. R. Zheng, Y. Tong, M. Zhang, G. Xu, C. Li, J. Ma and G. Shi, *ACS Energy Lett.*, 2018, **3**, 237–244.

33 Z. Xu, W. Li, Y. Yan, H. Wang, H. Zhu, M. Zhao, S. Yan and Z. Zou, *ACS Appl. Mater. Interfaces*, 2018, **10**, 22102−22109.

34 Z. Xing, Q. Li, D. Wang, X. Yang and X. Sun, *Electrochim. Acta*, 2016, **191**, 841–845.

35 Y. Zhu, H. A. Tahini, Z. Hu, J. Dai, Y. Chen, H. Sun, W. Zhou, M. Liu, S. C. Smith, H. Wang and Z. Shao, *Nat. Commun.*, 2019, **10**, 149.

36 C. Zhang, B. Chen, D. Mei and X. Liang, *J. Mater. Chem. A*, 2019, **7**, 5475–5481.

37 S. Palani, C. C. Liao, W. F. Chen, T. Chou, I. Shown, A. Sabbah, Y. G. Lin, J. F. Lee, M. K. Tsai, K. H. Chen and L. C. Chen, *J. Mater. Chem. A*, 2019, **7**, 7179–7185.

38 C. Wang, J. Li, S. Zhou, W. Cai, Z. Liu, J. Xiong, J. Liang, H. Cheng, Z. Yang and Z. Li, *J. Mater. Chem. A*, 2019, **7**, 5621–5625.

39 P. Zhou, B. Huang, P. Wang, X. Qin, D. Xing, X. Zhang, Y. Liu, Z. Wang, Z. Zheng and Y. Dai, *J. Mater. Chem. A*, 2019, **7**, 5513-5521.